Article

The GM1 Ganglioside Forms GM1-Rich Gel Phase Microdomains within Lipid Rafts

Lucia Becucci [1,*]**, Francesco Vizza** [1]**, Yolanda Duarte** [2] **and Rolando Guidelli** [2,†]

[1] Istituto di Chimica dei Composti Organo Metallici, Consiglio Nazionale delle Ricerche, Via Madonna del Piano 10, 50019 Sesto Fiorentino (Firenze), Italy;
E-Mail: francesco.vizza@iccom.cnr.it

[2] Department of Chemistry, Florence University, Sesto Fiorentino (Firenze) 50019, Italy;
E-Mails: yolandaduarte@hotmail.it (Y.D.); rolando.guidelli@libero.it (R.G.)

[†] Retired.

* Author to whom correspondence should be addressed; E-Mail: lucia.becucci@unifi.it;
Tel.: +39-55-4573-095; Fax: +39-55-4573-385.

Abstract: Mercury-supported, self-assembled monolayers (SAMs) of the sole dioleoylphosphatidylcholine (DOPC) and of a raft-forming mixture of DOPC, cholesterol (Chol) and palmitoylsphingomyelin (PSM) of (59:26:15) mol% composition, were investigated by electrochemical impedance spectroscopy (EIS), both in the absence and in the presence of the monosialoganglioside GM1. The impedance spectra of these four SAMs were fitted by a series of parallel combinations of a resistance and a capacitance (*RC* meshes) and displayed on plots of $\omega Z'$ against $-\omega Z''$, where Z' and Z'' are the in-phase and quadrature components of the impedance and ω is the angular frequency. A comparison among these different impedance spectra points to the formation of GM1-rich gel phase microdomains within the lipid rafts of the DOPC/Chol/PSM mixture, thanks to the unique molecular-level smooth support provided by mercury, which allows EIS to detect the protruding gel phase microdomains by averaging them over a macroscopically large area.

Keywords: lipid rafts; gel phase microdomains; electrochemical impedance spectroscopy; cholera toxin

1. Introduction

It is, nowadays, well established that binary lipid mixtures consisting of lipids with melting temperatures T_m, respectively, higher and lower than room temperature tend to undergo a phase separation, called demixing. Typically, gel phase microdomains enriched in the high-T_m component are surrounded by a liquid-crystalline phase enriched in the low-T_m component [1,2]. The gel phase is anisotropic, tightly packed, and has limited lateral mobility and axial rotation of the acyl chains. Conversely, the liquid-crystalline phase is isotropic, loosely packed and has a high degree of lateral mobility and axial rotation. Addition of cholesterol (Chol) to these binary mixtures has a disordering effect on the gel phase and an ordering effect on the liquid-crystalline phase. More precisely, in the liquid-crystalline phase cholesterol decreases axial rotation of acyl chains and, at concentrations above 30 mol%, it also decreases lateral diffusion. Conversely, Chol increases lateral diffusion and axial rotation in the gel phase microdomains, causing them to become isotropic [3]. This is revealed by a morphological investigation of these lipid mixtures by two-photon excitation fluorescence microscopy [4]. Thus, gel phase microdomains have irregular shapes due to their anisotropic structure. Conversely, the microdomains in the presence of Chol concentrations higher than about 6 mol% have a roundish shape, because they are isotropic like the surrounding liquid-crystalline phase. In this case, the line tension (the energy per unit length of the edge) associated with the edge of the two demixing phases tends to a minimum by optimizing the area-to-perimeter ratio. In other words, Chol causes the microdomains to pass from the gel phase to the so-called "liquid ordered" (l_o) phase. This phase is regarded as "liquid" thanks to its sufficient lateral diffusion, and "ordered" because it is more tightly packed than the liquid-crystalline phase, due to the still modest axial rotation of its acyl chains [3]. In contraposition with the l_o phase, the liquid-crystalline phase is often referred to as the "liquid disordered" (l_d) phase. Similarly, the gel phase is referred to as the solid ordered (s_o) phase. L_o microdomains, commonly referred to as lipid rafts, are thought to play a role in membrane organization, acting as platforms for the preferential sorting of proteins that interact with each other to carry out cellular functions, such as signal transduction. Coexistance of l_d and l_o phases has been observed and investigated on ternary biomimetic membranes composed of a saturated lipid, such as sphingomyelin (SM), an unsaturated lipid, such as dioleoylphosphatidylcholine (DOPC), and Chol.

Glycosphingolipids have been shown to exert a strong influence on phase separation in biomembranes, due to their long saturated acyl chains and bulky oligosaccharide hydrophilic headgroups [5]. These molecules are thought to localize in lipid rafts. The monosialoganglioside GM1 is an extensively investigated glycosphingolipid, which consists of a ceramide residue bound to a sugar chain containing an *n*-acetylneuraminic acid residue (see Chart 1). The sialic acid residue contains a carboxyl group that imparts to the polar head of GM1 a negative charge at pH 7. GM1 is present in the outer leaflet of plasma membranes of neurons, where it regulates axonal determination and growth, signaling and repair. It can be easily incorporated in biomimetic membranes and acts as a specific receptor of the cholera toxin (ChTo) [6,7]. This is an enterotoxin of *Vibrio cholerae*, composed of two subunits A and B of stoichiometry AB_5, which binds to GM1 via the B subunits [8,9].

SM/DOPC/Chol systems in the presence of GM1 have been investigated by fluorescence microscopy on giant unilamellar vesicles, as well as by several surface sensitive techniques, such as epifluorescence imaging, atomic force microscopy (AFM), mean-field scanning optical microscopy, synchrotron X-ray

reflectivity and secondary ion mass spectroscopy (SIMS). Fluorescence microscopy on giant unilamellar vesicles is a technique that may unequivocally discriminate l_o from s_o microdomains in a l_d matrix, by the use of appropriate fluorophores, such as laurdan [10]. Atomic force microscopy (AFM) at mica-supported lipid bilayers may detect changes in bilayer thickness and domain size [11–14]. X-ray reflectivity may provide useful information in terms of acyl chain and headgroup electron densities and bilayer thicknesses [15]. SIMS may provide distinct images of all components of a lipid mixture via isotopic labeling of each of them [16]. As a rule, measurements carried out by the above techniques point to a tendency of GM1 to be localized in the l_o phase of ternary DOPC/SM/Chol mixtures [10,12,14], due to repulsion between saturated and unsaturated acyl chains. Hydrogen bond formation between GM1 and SM, which are both hydrogen bond donors and acceptors, and of GM1 with Chol, which is a hydrogen bond donor, may also contribute to favor this tendency. However, AFM measurements at GM1 concentrations as high as 5 mol% also show a significant number of high microdomains, ascribable to the long GM1 molecules, in the DOPC-rich l_d matrix [12]. All surface sensitive techniques use lipid mono- or bilayers deposited on smooth supports, such as mica [11,12,14], silicon wafers [15], or silanized glass [10]. Lipid domains in the above solid supports may lack the reversible phase behavior characteristic of fluid membranes, and the domains can be pinned to the supports [15,17,18].

Chart 1. Primary structures of dioleoylphosphatidylcholine, cholesterol, palmitoylsphingomyelin and GM1 (proceeding downwards).
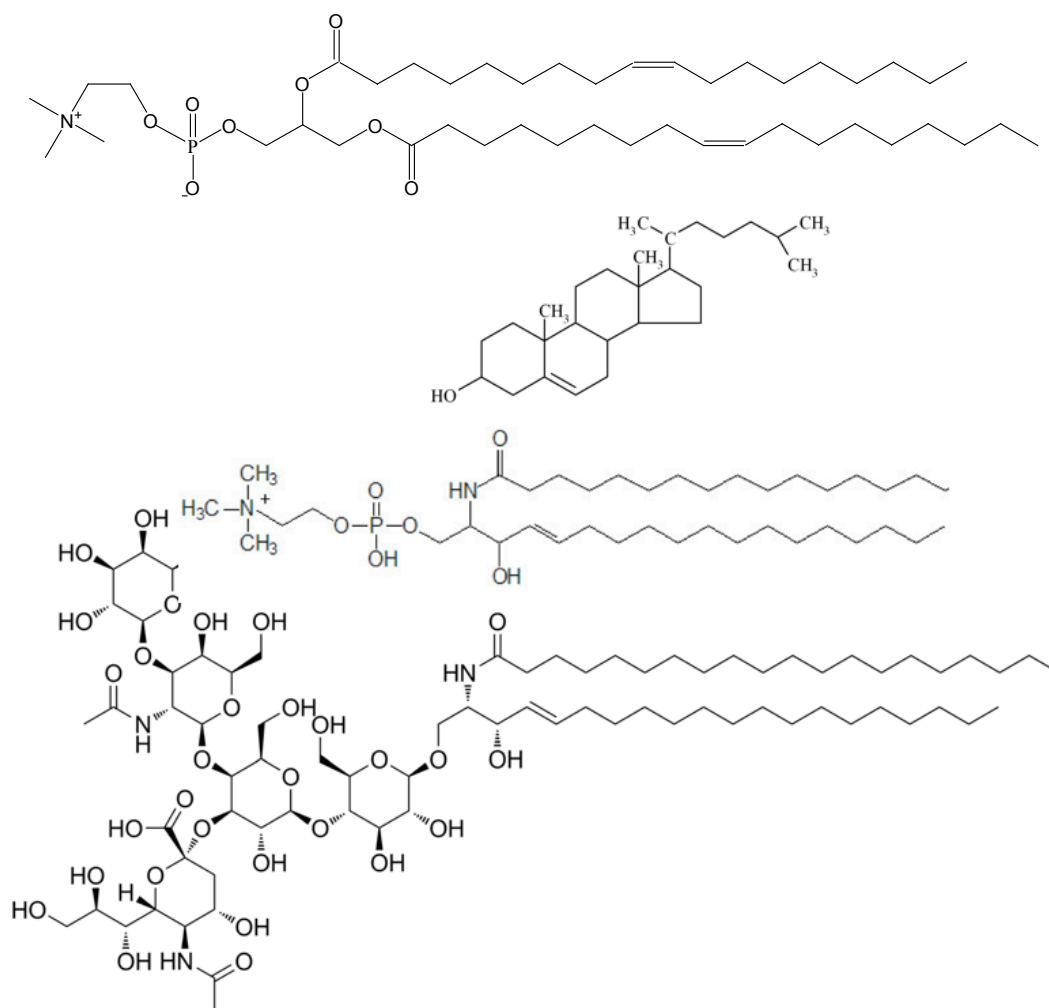
An advantage of mercury-supported lipid monolayers over solid-supported ones is represented by their fluidity and by a lateral mobility of the lipid molecules comparable to that of biomembranes, thanks to the liquid state of mercury [19]. Lipid molecules are readily self-assembled on the perfectly smooth mercury surface, with the hydrocarbon tails directed toward the metal and the polar heads turned toward the aqueous solution. Monolayers of lipid mixtures self-assembled on mercury form spontaneously gel-phase and l_o microdomains, thanks to the fluidity imparted to these monolayers by the liquid metal support [19]. In particular, monolayers of a binary mixture of a lipid component of high transition temperature T_m, such as palmitoylsphingomyelin (PSM), and of a low-T_m component, such as DOPC, form gel phase microdomains; these are typically enriched in the high-T_m component, and are surrounded by a l_d phase enriched in the low-T_m component [1,2]. The capacitance C_{ht} of the hydrocarbon tail region was found to increase in parallel with the amount of the gel phase in the mixture [19]. This behavior can be explained by assuming that C_{ht} is approximately proportional to the total perimeter of the edge of the gel phase microdomains. Following an AC signal, inorganic ions can move more easily back and forth along the mismatch between anisotropic gel phase microdomains and the surrounding isotropic l_d matrix, causing an increase in differential capacitance. Addition of Chol to binary mixtures of a low-T_m and a high-T_m component removes this mismatch, converting gel-phase microdomains into lipid rafts and decreasing the differential capacitance accordingly [19]. We, therefore, found it interesting to investigate the effect of the addition of 20 mol% GM1 to mercury-supported monolayers consisting either of pure DOPC or of a raft-forming lipid mixture, by using electrochemical impedance spectroscopy (EIS).

2. Materials and Methods

2.1. Materials

The water used was obtained from water produced by an inverted osmosis unit, upon distilling it once and then distilling the water so obtained from alkaline permanganate. Merck (Milano, Italy) suprapur® KCl was baked at 500 °C before use to remove any organic impurities. Palmitoylsphingomyelin (PSM) and dioleoylphosphatidylcholine (DOPC) were purchased in chloroform solution from Avanti Polar Lipids (Birmingham, AL, USA). Cholesterol (Chol) and cholera toxin B subunit (ChTo B) were purchased from Sigma (Milano, Italy) and used without further purification.

2.2. Preparation of Mercury-Supported Self-Assembled Monolayers (SAMs)

Mercury-supported lipid self-assembled monolayers (SAMs) were obtained by spreading an amount of lipid solution in pentane, corresponding to about 2.5 lipid monolayers, on the surface of an aqueous solution of 0.1 M KCl and allowing the pentane to evaporate. A homemade hanging mercury drop electrode (HMDE) was then immersed into the aqueous solution across the lipid film using an oleo-dynamic system. This procedure gives rise to a lipid monolayer with the hydrocarbon tails directed toward the mercury surface, thanks to its hydrophobic nature [20–22]. This lipid self-assembly is equivalent to a Langmuir-Blodgett transfer at the equilibrium spreading pressure [23]. In fact, by spreading an excess of the lipid at the nitrogen/solution interface, one obtains a monolayer at the characteristic spreading pressure (about 45 mN/m²), in equilibrium with the bulk phase of the surfactant,

i.e., a floating crystal of the surfactant [23–25]. The composition of the lipid monolayer self-assembled on a mercury drop through its passage across the lipid monolayer spread on the surface of the working solution is expected to be practically the same as that of the latter lipid monolayer, in analogy with Langmuir-Blodgett transfer. In fact, the dipping speed employed, 0.4 cm/s, prevents the lipid monolayer coating the mercury drop from varying its composition during the very short time in which it remains in contact with the lipid monolayer spread on the solution surface.

2.3. Instrumentation

Electrochemical measurements on lipid-coated mercury were carried out in aqueous 0.1 M KCl. Use was made of a home-made HMDE described elsewhere [26]. A home-made glass capillary with a finely tapered tip, about 1 mm in outer diameter, was employed. Capillary and mercury reservoir were thermostated at 25 ± 0.1 °C in a water-jacketed box to avoid any changes in drop area due to a change in temperature. EIS measurements were carried out over the frequency range from 0.1 to 1×10^5 Hz with an Autolab instrument PGSTAT 12 (Echo Chemie, Utrecht, The Netherlands) supplied with FRA2 module for impedance measurements, SCAN-GEN scan generator and GPES 4.9005 Beta software. Potentials were measured *vs.* an Ag/AgCl electrode immersed in the 0.1 M KCl working solution.

3. Results

Lipid monolayers consisting either of pure DOPC or of a DOPC/Chol/PSM mixture of (59:26:15) mol% composition, typical of mammalian plasma membranes, were examined by EIS, both before and after addition of 20 mol% GM1 to both these monolayers. In what follows, the DOPC/Chol/PSM (59:26:15) mixture will be denoted by DCP, for simplicity. According to the phase diagram of the (palmitoyloleoylphosphatidylcholine:POPC)/Chol/PSM lipid mixture estimated by de Almeida *et al.* [27,28], the (59:26:15) mol% composition adopted herein falls in the middle of the $l_o + l_d$ phase coexistence region. This result can be safely extended to the DOPC/Chol/PSM (59:26:15) mixture, since the two low-T_m components DOPC and POPC are expected to exhibit practically the same behavior. The DOPC/Chol/PSM/GM1 mixture of (47:21:12:20) mol% composition will be briefly denoted by DCP/GM1. Measurements were carried at −0.55 V. The choice of this potential was dictated by its falling in the middle of the range of stability of Hg-supported lipid monolayers. Thus, the maximum value of the film pressure of a Hg-supported DOPC monolayer in 0.1 M KCl falls at about −0.48 V, which is equivalent to the potential of maximum stability of the lipid monolayer relative to its displacement by water [24].

The impedance spectra are displayed on a $\omega Z'$ *versus* $-\omega Z''$ plot, where ω is the angular frequency and Z', Z'' are the in-phase and quadrature components of the electrochemical impedance. To interpret impedance spectra, it is necessary to compare them with the electrical response of an equivalent circuit simulating the system under investigation. In this respect, a metal-supported self-assembled monolayer (SAM) can be conveniently regarded as consisting of a series of slabs with different dielectric properties. In an equivalent circuit, a dielectric slab can be represented as a resistance and a capacitance in parallel, namely an *RC* mesh. Therefore, an impedance spectrum can be fitted by an equivalent circuit consisting of a series of *RC* meshes. In a $\omega Z'$ *versus* $-\omega Z''$ plot, which will be briefly referred to as a M plot (where M stands for modulus), a single *RC* mesh yields a semicircle of diameter $1/C$; the angular frequency at

the maximum of the semicircle equals the reciprocal of the time constant, RC, of the mesh [19]. If the time constants of the different dielectric slabs are too close, the corresponding semicircles may overlap to an appreciable extent, making their resolution relatively inaccurate. Since the frequency increases along the positive direction of the $-\omega Z''$ axis, the partially overlapping semicircles are aligned in the order of decreasing time constant, when proceeding in this direction. Thus, for a series of RC meshes, the last semicircle on the right hand side of an M plot is characterized by the lowest time constant.

The number of RC meshes simulating the different slabs of a biomimetic membrane is not uniquely defined. One can try to increase their number as long as it is reasonably possible to separate their contributions, which tend to overlap the more the higher this number is. With SAMs of DOPC, DCP and DOPC/GM1, the minimum number of RC meshes simulating the impedance spectrum, with fitting errors less than 10%, was found to be four; a further increase in this number was found not to improve the fitting. The four RC meshes are considered to simulate (i) the hydrocarbon tail region, (ii) the polar head region, (iii) the diffuse layer, and (iv) the aqueous solution bathing the lipid monolayer. Their time constants, which decrease in the above order, will be denoted by $R_{ht}C_{ht}$, $R_{ph}C_{ph}$, $R_{dl}C_{dl}$ and $R_\Omega C_\Omega$. In particular, the hydrocarbon tail region has the highest resistance, R_{ht}.

In an aqueous solution of 0.1 M KCl, the capacitance C_Ω and resistance R_Ω of the aqueous solution assume values of about 35 nF·cm^{-2} and 3.5 Ω·cm^2, respectively, and are clearly independent of the particular lipid SAM. These two values yield the lowest time constant, $C_\Omega R_\Omega$, which, as such, gives rise to the very large semicircle on the right-hand side of the M plot. In practice, over the frequency range covered by the EIS instrumentation, only a small portion of this very large semicircle, $1/C_\Omega$ in diameter, is visible in the M plot. The diffuse layer has also a low time constant, having a resistance, R_{dl}, of the order of 1 Ω·cm^2 but a much higher capacitance, C_{dl}, of about 70 μF·cm^{-2}. The latter value is close to the capacitance expressed by the Gouy-Chapman theory for the aqueous solution of a 1,1-valent electrolyte in contact with an uncharged surface. This result is expected, since the DOPC is neutral and the charge density on the surface of the mercury electrode over the potential range of stability of a lipid SAM ranges from −0.2 to −1.3 μC cm^{-2} [24]. The accuracy in the estimate of R_{dl} and C_{dl} is low, because the RC mesh ascribable to the diffuse layer straddles the maximum frequency covered by the EIS instrumentation. Thus, the difference between the fit that includes the $R_{dl}C_{dl}$ mesh and that which neglects it can only be appreciated over the frequency range from 10^4 and 10^5 Hz and amounts to a maximum of +30% for the DCP/GM1 SAM and of +20% for the DOPC/GM1 SAM. For the other two SAMs it is smaller and comparable with the range of the experimental error.

The M plots for the DOPC, DCP and DOPC/GM1 monolayer are shown in Figures 1, 2, and 3, respectively. In these figures, the calculated contribution to $\omega Z'$ from each single RC mesh is plotted against the overall $-\omega Z''$ quantity. This serves to show how each semicircle is affected by partial overlapping with the neighboring ones. Each contribution is represented by a semicircle that is distorted the more, the higher the overlapping. The contributions to $\omega Z'$ against $-\omega Z''$ are represented in blue for the hydrocarbon tails, in red for the polar heads, in brown for the diffuse layer and in green for the aqueous solution. The relatively flat M plot in Figure 4 for the DCP/GM1 monolayer required a further RC mesh for the fitting, in addition to the four RC meshes employed for the other lipid SAMs; its significance will be examined in Section 4. The R and C values for all RC meshes of the four lipid SAMs are reported in the legends for the corresponding figures; the values for the two RC meshes ascribable to the hydrocarbon tails and the polar heads of the monolayers of DOPC, DCP, DOPC/GM1 and

DCP/GM1 are plotted in Figure 5, in the above order, to evidence possible trends. The capacitance of the hydrocarbon tails of the DOPC SAM, $C_{ht} = 1.9$ µF·cm^{-2}, is about twice that, between 0.9 and 1 µF·cm^{-2}, of solvent-free bilayer lipid membranes and in good agreement with the value of 1.80 µF·cm^{-2}, reported by Nelson [21].

Addition of 10 nM ChTo B to the aqueous solution bathing the lipid monolayers that incorporate GM1 has a negligible effect on their impedance spectra, even after an incubation time of 1 h.

Figure 1. Plot of $\omega Z'$ against $-\omega Z''$ for a Hg-supported DOPC monolayer in aqueous 0.1 M KCl at -0.550 V. Solid circles are experimental points and the black curve is the best fit to these points by a series of four RC meshes. The contributions to $\omega Z'$ against $-\omega Z''$ are represented in blue for the hydrocarbon tails, in red for the polar heads, in brown for the diffuse layer, and in green for the aqueous solution. Capacitances and resistances of the four RC meshes are: $R_{ht} = 3.3$ MΩ·cm^2, $C_{ht} = 1.9$ µF·cm^{-2}, $R_{ph} = 3.6$ kΩ·cm^2, $C_{ph} = 51$ µF·cm^{-2}, $R_{dl} = 1$ Ω·cm^2, $C_{dl} = 70$ µF·cm^{-2}, $R_\Omega = 4.2$ Ω·cm^2, $C_\Omega = 36$ nF·cm^{-2}. The impedance spectrum in the inset covers a broader frequency range encompassing the contribution from the aqueous solution.
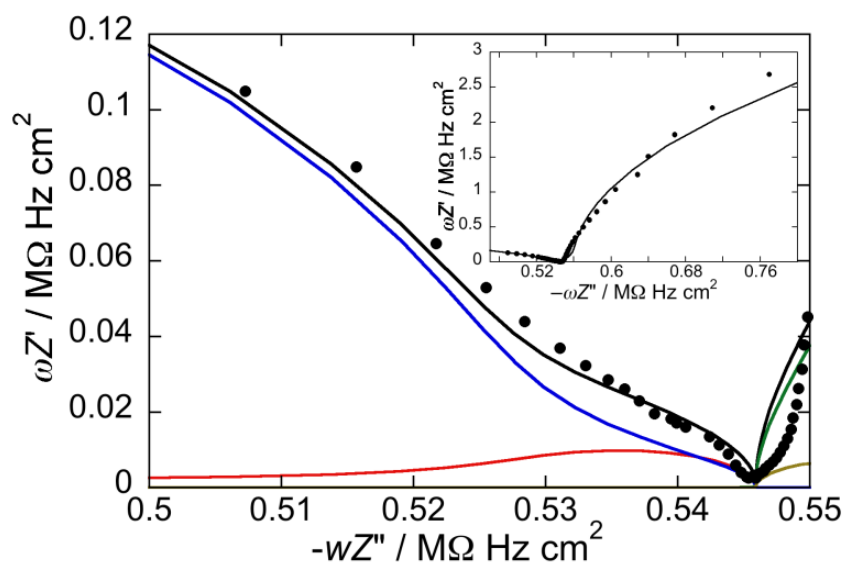
4. Discussion

Figure 5 shows the changes in capacitance and resistance of the hydrocarbon tails and polar heads along the DOPC, DCP, DOPC/GM1, DCP/GM1 sequence. The C_{ht} values increase roughly linearly along this sequence from 1.9 to 6 µF·cm^{-2}. This behavior may be explained by the gradual increase in the heterogeneity of the mixture of kinked unsaturated and linear saturated hydrocarbon tails decreasing the lipid packing; this facilitates the penetration of small inorganic ions among these tails and an increase in the amount of back and forth movement along them following the AC voltage signal, with a resulting increase in C_{ht}. The resistance, R_{ht}, of the hydrocarbon tails ranges between 1.5 and 3.5 MΩ·cm^2 for all lipid SAMs, except for the DCP mixture, whose R_{ht} value is smaller by more than one order of magnitude. The behavior of the DCP SAM differs notably from that of the other three SAMs even with respect to the polar heads. Thus, the C_{ph} and R_{ph} values for the DOPC, DOPC/GM1 and DCP/GM1

SAMs are around 50–55 $\mu F \cdot cm^{-2}$ and 3.5–5.5 $k\Omega \cdot cm^2$, respectively, whereas C_{ph} for DCP is one order of magnitude smaller and the corresponding R_{ph} value one order of magnitude higher. In practice, the capacitance of the polar head region of DCP is very close to that of the hydrocarbon tail region.

The low C_{ph} value and high R_{ph} value for DCP with respect to those for the other three SAMs is probably to be ascribed to a network of hydrogen bonds of the PSM molecules both between themselves and with Chol molecules; this contributes to stiffening the polar heads. In particular, molecular dynamics simulations of SM/Chol mixtures predict strong hydrogen bonds of the hydroxyl group of Chol with the ceramide functional group and the phosphate group of PSM, whereas SM-SM hydrogen bonds are weak and Chol-Chol ones are hardly observed [29]. The Chol molecules, with their short, rigid and compact tetracyclic ring structure, span only the distal portion of the lipid monolayer, with their hydroxyl groups forming hydrogen bonds with the PSM polar heads. Thus, on the one hand they create an interstitial space available for ion movement below their small tails, increasing C_{ht}, and on the other hand they contribute to stiffening the polar head region, decreasing C_{ph} and increasing R_{ph}. In practice, in the DCP SAM, the extent of back and forth movement of small inorganic ions along the polar heads matches that along the hydrocarbon tails.

Figure 2. Plot of $\omega Z'$ against $-\omega Z''$ for a Hg-supported DOPC/Chol/PSM (59:26:15) mol% monolayer in aqueous 0.1 M KCl at -0.550 V. Solid circles are experimental points and the black curve is the best fit to these points by a series of four *RC* meshes. The contributions to $\omega Z'$ against $-\omega Z''$ are represented in blue for the hydrocarbon tails, in red for the polar heads, in brown for the diffuse layer, and in green for the aqueous solution. Capacitances and resistances of the four *RC* meshes are: $R_{ht} = 0.13$ $M\Omega \cdot cm^2$, $C_{ht} = 3.7$ $\mu F \cdot cm^{-2}$, $R_{ph} = 50$ $k\Omega \cdot cm^2$, $C_{ph} = 3.3$ $\mu F \cdot cm^{-2}$, $R_{dl} = 0.9$ $\Omega \cdot cm^2$, $C_{dl} = 50$ $\mu F \cdot cm^{-2}$, $R_\Omega = 3.8$ $\Omega \cdot cm^2$, $C_\Omega = 38$ $nF \cdot cm^{-2}$. The impedance spectrum in the inset covers a narrower frequency range.
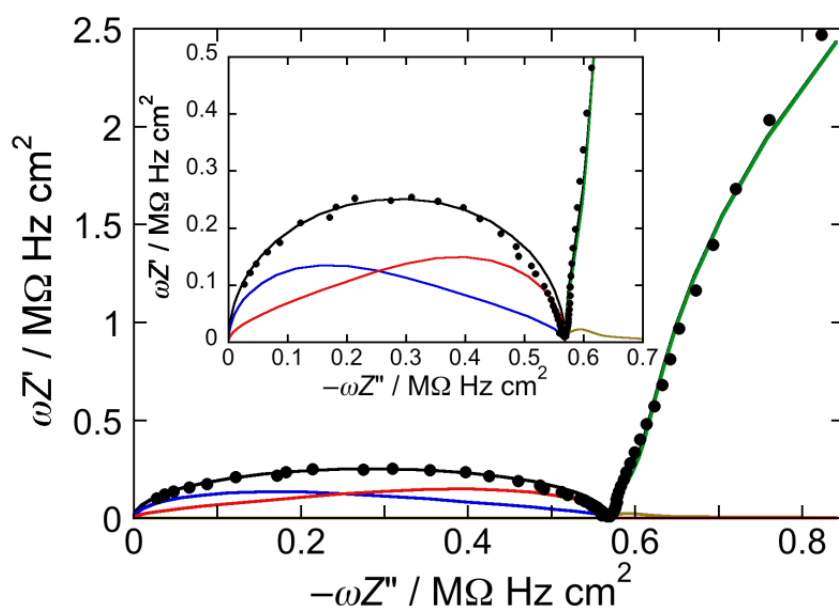
Figure 3. Plot of $\omega Z'$ against $-\omega Z''$ for a Hg-supported DOPC/GM1 (80:20) mol% monolayer in aqueous 0.1 M KCl at -0.550 V. Solid circles are experimental points and the black curve is the best fit to these points by a series of four RC meshes. The contributions to $\omega Z'$ against $-\omega Z''$ are represented in blue for the hydrocarbon tails, in red for the polar heads, in brown for the diffuse layer, and in green for the aqueous solution. Capacitances and resistances of the four RC meshes are: $R_{ht} = 3.2$ M$\Omega \cdot$cm^2, $C_{ht} = 4.6$ μF$\cdot$cm^{-2}, $R_{ph} = 5.5$ k$\Omega \cdot$cm^2, $C_{ph} = 54$ μF$\cdot$cm^{-2}, $R_{dl} = 0.3$ $\Omega \cdot$cm^2, $C_{dl} = 70$ μF$\cdot$cm^{-2}, $R_{\Omega} = 3.2$ $\Omega \cdot$cm^2, $C_{\Omega} = 25$ nF$\cdot$cm^{-2}. The impedance spectrum in the inset covers a broader frequency range encompassing the contribution from the aqueous solution.
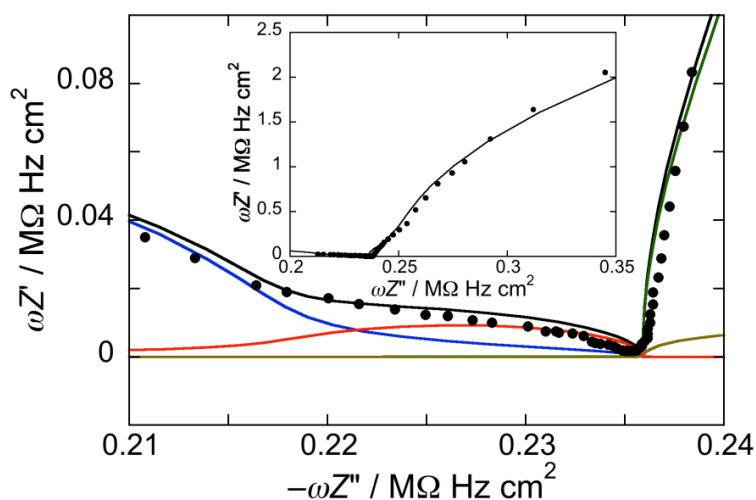
Figure 4. Plot of $\omega Z'$ against $-\omega Z''$ for a Hg-supported DOPC/Chol/PSM/GM1 (47:21:12:20) mol% monolayer in aqueous 0.1 M KCl at -0.550 V. Solid circles are experimental points and the black curve is the best fit to these points by a series of five RC meshes. The contributions to $\omega Z'$ against $-\omega Z''$ are represented in blue for the hydrocarbon tails, in red for the polar heads, in brown for the diffuse layer, in green for the aqueous solution, and in violet for an additional $R_{il}C_{il}$ mesh, ascribed to the "inner layer". Capacitances and resistances of the five RC meshes are: $R_{ht} = 1.6$ M$\Omega \cdot$cm^2, $C_{ht} = 6.1$ μF cm^{-2}, $R_{ph} = 3.4$ k$\Omega \cdot$cm^2, $C_{ph} = 57$ μF$\cdot$cm^{-2}, $R_{dl} = 1.6$ $\Omega \cdot$cm^2, $C_{dl} = 73$ μF$\cdot$cm^{-2}, $R_{\Omega} = 3.5$ $\Omega \cdot$cm^2, $C_{\Omega} = 27$ nF$\cdot$cm^{-2}, $R_{il} = 50$ $\Omega \cdot$cm^2, $C_{il} = 90$ μF$\cdot$cm^{-2}.
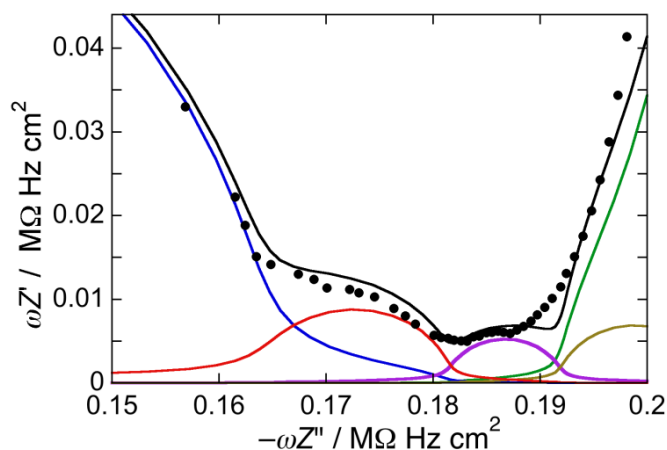
Figure 5. Capacitance and resistance of hydrocarbon tails and polar heads along the DOPC, DCP, DOPC/GM1, DCP/GM1 sequence.
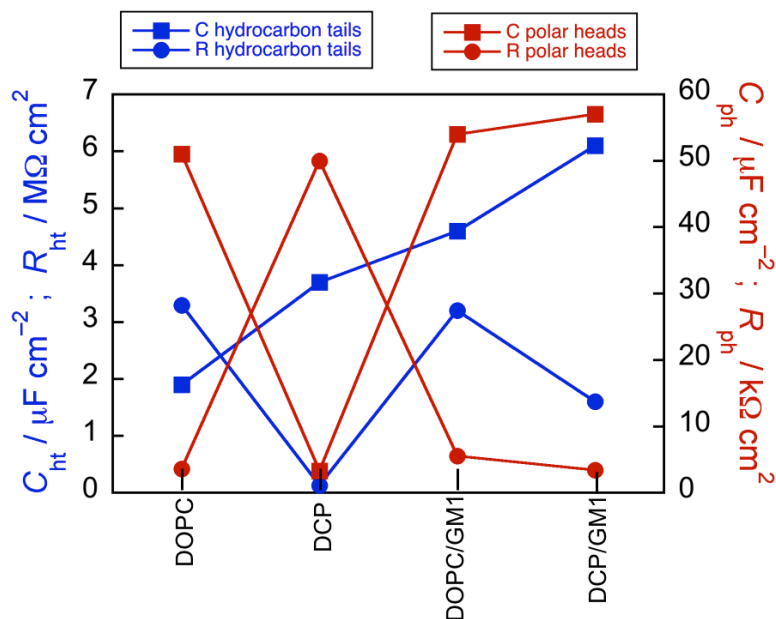
It should be noted that the PSM molecules are longer than the DOPC molecules. For the purpose of EIS analysis, we can imagine subdividing the polar head region into two ideal slabs parallel to the mercury surface. The slab closer to the electrode surface contains the polar heads of the shorter lipid (*i.e.*, DOPC) as well as the distal portion of the hydrocarbon tails of the longer lipid (*i.e.*, PSM). The outer slab contains the polar heads of the PSM molecules intercalated with the water molecules. The presence of this further slab does not yield an additional *RC* mesh in the impedance spectrum. This indicates that the PSM molecules are highly dispersed among the water molecules, in the form of single monomers or small aggregates. In this case, the high dielectric constant of water imparts to this slab a high capacitance and a low resistance, making it practically invisible to EIS. In fact, EIS is sensitive to the static dielectric constant, which equals 80 for water and is of the order of 2 for lipid hydrocarbon tails. Hence, it can hardly distinguish a highly hydrated layer from the aqueous solution [30].

This behavior should be compared with that of Hg-supported DOPC/PSM SAMs with mol% PSM $\geq$ 20, which are known to form PSM-rich gel phase microdomains [19,27,28]. The impedance spectra of these SAMs require the addition of a further *RC* mesh of capacitance 35 $\pm$ 10 µF·cm^{-2} and resistance 250 $\pm$ 50 Ω·cm^2 for a satisfactory fit [19]. This indicates that, when the PSM molecules are aggregated into sufficiently large and compact microdomains, the dielectric slab consisting of clusters of the protruding PSM polar heads intercalated with water molecules can be detected by EIS. The capacitance of such a slab is expressed by the sum of the capacitance of the clusters of PSM polar heads and that of the water molecules, each multiplied by the corresponding mole fraction, provided edge effects are negligible. The local value of the diffuse layer capacitance in close contact with the microdomains does not necessarily coincide with that predicted by the Gouy-Chapman theory. A numerical estimate of this quantity near ultramicroelectrodes yields values as high as 200 µF cm^{-2} [31]. Thus, we cannot exclude capacitance values of the water molecules around the asperities represented by gel-phase microdomains appreciably higher than those on the flat l$_d$ matrix.

It should be noted that the analysis of the impedance spectra of Hg-supported lipid SAMs does not reveal the presence of an additional *RC* mesh if the SAM contains l_o microdomains (*i.e.*, lipid rafts) but no gel phase microdomains. This is the case with the DCP SAM examined in this work. Only the presence of gel phase microdomains provides evidence for an additional *RC* mesh in the fitting of the impedance spectrum. This is because the detection of an additional *RC* mesh by EIS requires that tightly packed microdomains with a low content of water protrude out of the l_d matrix. This requirement is not fulfilled by lipid rafts. The detection of an additional *RC* mesh also requires a molecular level smooth support, such as that provided by the liquid mercury surface, because the protrusion of the gel phase microdomains must be averaged over a macroscopically large area. On solid supports such as mica, a difference in height between gel phase microdomains and the surrounding matrix can only be detected at nanoscale distances along the surface, e.g., by AFM.

Addition of 20 mol% GM1 to the DCP mixture restores a capacitance C_{ph} close to that for the DOPC and DOPC/GM1 SAMs, thus, disrupting the Chol-PSM hydrogen bonds (see Figure 5). This behavior can be understood by considering that a satisfactory fit of the impedance spectrum of the DCP/GM1 SAM requires an additional *RC* mesh of capacitance 90 ± 10 $\mu F \cdot cm^{-2}$ and a resistance of about 50 $\Omega \cdot cm^2$. The features of this *RC* mesh are similar to those of the additional *RC* mesh reported for Hg-supported DOPC/PSM SAMs with mol% PSM > 20 [19], which are known to form PSM-rich gel phase microdomains. The *RC* mesh for the DCP/GM1 SAM can be likewise ascribed to GM1-rich gel phase microdomains. The electrostatic repulsion between the negatively charged oligosaccharide headgroups of GM1 and the steric hindrance of its bulky sugar and sialic acid groups can hardy allow the formation of pure GM1 microdomains. The strong hydrogen bonds between the hydroxyl groups and the amide carbonyl groups of the ceramide moieties of GM1 and PSM and, even more so, between PSM and the β-D-glucose and β-D-galactose residues of the GM1 headgroup [29] strongly suggest the recruitment of PSM molecules by the GM1-rich microdomains. This is more likely to occur within the PSM-rich lipid rafts, which exist prior to the addition of GM1. This process induces the breaking of the hydrogen bonds between PSM and Chol molecules. On the other hand, the presence of Chol molecules in the GM1-rich gel-phase microdomains is expected to be low. In fact, a significant Chol content in the gel phase microdomains would convert them into lipid rafts, eliminating the mismatch at the boundary between the anisotropic gel phase microdomains and the surrounding l_d matrix.

These conclusions are in agreement with an AFM study of GM1 domains in DCP monolayers on mica. AFM images of DOPC/Chol/PSM (1:1:1) mol% monolayers show microdomains higher then the surrounding l_d matrix by about 1.0 nm, ascribable to the l_o phase [12]. In the presence of GM1, numerous bright dots randomly distributed in the l_o phase are observed, approximately 1.0 nm higher than the latter phase. For GM1 mole fractions higher than 5%, these dots coalesce to form a complex network of filaments. Both dots and filaments are assigned to a GM1-rich phase. Fluorescent confocal microscopy measurements on giant unilamellar vesicles of identical composition show that the l_o domains are enriched with fluorescently labeled GM1 and PSM, while fluorescently labeled dioleoylphosphatidylethanolamine (DOPE) is almost absent in these domains [32]; however, GM1 and PSM are not completely absent in the l_d phase. A monolayer of GM1/DMPC(dimyristoylphosphatidylcholine)/Chol with mole ratios of 1:6:3, 2:5:3 and 3:4:3 was investigated by Lipkowski and coworkers by AFM [33]. This monolayer constituted the inner leaflet of a bilayer lipid membrane floating on top of a hydrophilic monolayer of thioglucose anchored to Au(111) and separated from this metal support by a 2-nm water-rich region; the

outer leaflet was composed of a 7:3 mole ratio of DMPC/Chol. The 10 and 30 mol% GM1 leaflets are uniform and smooth, with the 30 mol% one probably in a condensed state. Conversely, the 20 mol% GM1 film is phase-separated, with a GM1-rich phase elevated by approximately 1 nm with respect to the surrounding DMPC-rich l_d phase.

The absence of an additional *RC* mesh in the impedance spectrum of the DOPC/GM1 SAM, as distinct from the DCP/GM1 SAM, excludes the presence of GM1-rich gel phase microdomains in a DOPC l_d matrix and strongly suggests a random distribution of GM1 molecules in the DOPC monolayer. This conclusion agrees with freeze-etch electron microscopy [34] and differential scanning calorimetry [35] investigations of model membranes, according to which mixtures of low-T_m phosphatidylcholines (PCs) with small quantities of GM1 suggest that GM1 is completely miscible with these PCs in the l_d phase. It is also in keeping with molecular dynamics simulations on GM1/SM/Chol and GM1/POPC lipid bilayers [29]. These simulations show that the GM1 molecules in the GM1/SM/Chol membrane are condensed, with numerous hydrogen bonds among glycan portions of the GM1 clusters, whereas those in the GM1/POPC membrane are scattered. In other words, the formation of GM1 aggregates is observed only on the GM1/SM/Chol mixed membrane. Yuan and Johnston [11] report small domains of variable size (50–100 nm) and height in GM1/egg PC (5:95) mol% mixtures on mica by AFM. However, the amount of GM1 in the DOPC-rich phases increases with both increasing surface pressure (in our SAMs, 45 mN/m^2) and GM1 concentration [12,13]. Moreover, a combination of two-color fluorescence and AFM, which allows a distinction between monomeric and aggregated GM1, reveals the presence of monomeric GM1 units in the l_o phase of DOPC/DPPC monolayers [13].

In spite of the appreciable difference between the behavior of 20 mol% GM1 in raft-making lipid monolayers and in pure DOPC monolayers, addition of 10 nM ChTo B has no detectable effect on the impedance spectra of these monolayers. This behavior is in apparent contrast with surface plasmon resonance (SPR) measurements recently carried out by two of us and others on DOPC/GM1 and DCP/GM1 floating bilayers self-assembled on a hydrophilic thiol tethered to a gold slide [36]. SPR angular spectra at a DCP/GM1 bilayer in aqueous solution of 10 nM ChTo B monitored an optical thickness about twice that at a DOPC/GM1 bilayer. This points to a marked preference of ChTo B for binding to GM1-rich microdomains with respect to GM1 monomers, at constant GM1 mole fraction in the lipid mixture. This apparent discrepancy is to be ascribed to a considerable amount of water in ChTo B molecules on supported lipid layers [30,37]. The presence of this large amount of water makes the protein layer bound to GM1 practically invisible to EIS. Conversely, the optical response is proportional to the actual mass coverage, independent of its water content [30].

5. Conclusion

The different behavior of GM1 incorporated in a lipid monolayer self-assembled on mercury, depending on whether the monolayer consists of a pure low-T_m lipid or of a raft-forming mixture, points to the formation of GM1-rich gel phase microdomains located in the l_o phase of the latter mixture. The unique molecular-level smooth support provided by mercury allows electrochemical impedance spectroscopy to detect the protruding gel phase microdomains by averaging them over a macroscopically large area.

Acknowledgments

Author Contributions

L. B. organized the research, carried out a part of EIS measurements and analyzed the impedance spectra on the basis of the appropriate equivalent circuit, F. V. carried out another part of EIS measurements, R. G. wrote the manuscript and Y. D. improved the use of English in the manuscript.

Conflicts of Interest

The authors declare no conflict of interest.

References

1. Brown, D.A.; London, E. Structure and origin of ordered lipid domains in biological membranes. *J. Membr. Biol.* **1998**, *164*, 103–114.
2. Brown, D.A.; London, E. Structure and function of sphingolipid- and cholesterol-rich rafts. *J. Biol. Chem.* **2000**, *275*, 17221–17224.
3. Parasassi, T.; Giusti, A.M.; Raimondi, M.; Gatton, E. Abrupt modifications of phospholipid bilayer properties at critical cholesterol concentrations. *Biophys. J.* **1995**, *68*, 1895–1902.
4. Bagatolli, L.A. To see or not to see: Lateral organization of biological membranes and fluorescent microscopy. *Biochim. Biophys. Acta* **2006**, *1758*, 1541–1556.
5. Schnaar, R.L.; Suzuki, A.; Stanley, P. Glycosphingolipids. In *Essentials of Glycobiology*, 2nd ed., Varki, A., Cummings, R.D., Esko, J.D., Freeze, H.H., Stanley, P., Bertozzi, C.R., Hart, G.W., Etzer, M.E., Eds.; Cold Spring Harbor Laboratory Press: New York, NY, USA, 2009.
6. Cuatrecasas, P. Interaction of Vibrio cholerae enterotoxin with cell membranes. *Biochemistry* **1973**, *12*, 3547–3558.
7. Holmgren, J.; Lönnroth, I.; Månsson, J.-E.; Svennerholm, L. Interaction of cholera toxin and membrane GM1 ganglioside of small intestine. *Proc. Nat. Acad. Sci. USA* **1975**, *72*, 2520–2524.
8. LoSpalluto, J.J.; Finkelstein, R.A. Chemical and physical properties of cholera exo-enterotoxin (choleragen) and its spontaneously formed toxoid (choleragenoid). *Biochim. Biophys. Acta* **1972**, *257*, 158–166.
9. Lönnroth, I.; Holmgren, J. Subunit structure of cholera toxin. *J. Gen. Microbiol.* **1973**, *76*, 417–427.
10. Dietrich, C.; Bagatolli, L.A.; Volovyk, Z.N.; Thompson, N.L.; Levi, M.; Jacobson, K.; Gratton, E. Lipid rafts reconstited in model membranes. *Biophys. J.* **2001**, *80*, 1417–1428.
11. Yuan, C.; Johnston, L.J. Atomic force microscopy studies of ganglioside GM1 domains in phosphatidylcholine and phosphatidylcholine/cholesterol bilayers. *Biophys. J.* **2001**, *81*, 1059–1069.
12. Yuan, C.; Furlong, J.; Burgos, P.; Johnston, L.J. The size of lipid rafts: An atomic force microscopy study of ganglioside GM1 domains in sphingomyelin/DOPC/cholesterol membranes. *Biophys. J.* **2002**, *82*, 2526–2535.

13. Coban, O.; Burger, M.; Laliberte, M.; Ianoul, A.; Johnston, L.J. Ganglioside partitioning and aggregation in phase-separated monolayers characterized by Bodipy GM1 monomer/dimer emission. *Langmuir* **2007**, *23*, 6704–6711.
14. Bao, R.; Li, L.; Qiu, F.; Yang, Y. Atomic force microscopy study of ganglioside GM1 concentration effect on lateral phase separation of sphingomyelin/dioleoylphosphatidylcholine/cholesterol bilayers. *J. Phys. Chem. B* **2011**, *115*, 5923–5929.
15. Reich, C.; Horton, M.R.; Krause, B.; Gast, A.P.; Rädler, J.O.; Nickel, B. Asymmetric structural features in single supported lipid bilayers containing cholesterol and GM1 resolved with synchrotron X-ray reflectivity. *Biophys. J.* **2008**, *95*, 657–668.
16. Lozano, M.M.; Liu, Z.; Sunnik, E.; Janshoff, A.; Kumar, K.; Boxer, S.G. Colocalization of the ganglioside GM1 and cholesterol detected by secondary ion mass spectrometry. *J. Am. Chem. Soc.* **2013**, *135*, 5620–5630.
17. Stottrup, B.L.; Veatch, S.L.; Keller, S.L. Nonequilibrium behavior in supported lipid membranes containing cholesterol. *Biophys. J.* **2004**, *86*, 2942–2950.
18. Mao, Y.; Shang, Z.; Imai, Y.; Hoshino, T.; Tero, R.; Tanaka, M.; Yamamoto, N.; Yanagisawa, K.; Urisu, T. Surface-induced phase separation of a sphingomyelin/cholesterol/ganglioside GM1-planar bilayer on mica surfaces and microdomain molecular conformation that accelerates Aβ oligomerization. *Biochim. Biophys. Acta* **2010**, *1798*, 1090–1099.
19. Becucci, L.; Martinuzzi, S.; Monetti, E.; Mercatelli, R.; Quercioli, F.; Battistel, D.; Guidelli, R. Electrochemical impedance spectroscopy and fluorescence lifetime imaging of lipid mixtures self-assembled on mercury. *Soft Matter* **2010**, *6*, 2733–2741.
20. Nelson, A.; Benton, A. Phospholipid monolayers at the mercury/water interface. *J. Electroanal. Chem.* **1986**, *202*, 253–270.
21. Nelson, A. Electrochemistry of mercury supported phospholipid monolayers and bilayers. *Curr. Opin. Colloid Interface Sci.* **2010**, *15*, 455–466.
22. Moncelli, M.R.; Becucci, L.; Nelson, A.; Guidelli, R. Electrochemical modelling of electron and proton transfer to ubiquinone-10 in a self-assembled phospholipid monolayer. *Biophys. J.* **1996**, *70*, 2716–2726.
23. Bizzotto, D.; Yang, Y.; Shepherd, J.L.; Stoodley, R.; Agak, J.; Stauffer, V.; Lathuillière, M.; Akhtar, A.S., Chung, E. Electrochemical and spectroelectrochemical characterization of lipid organization in an electric field. *J. Electroanal. Chem.* **2004**, *574*, 167–184.
24. Bizzotto, D.; Nelson, A. Continuing electrochemical studies of phospholipid monolayers of dioleoyl phosphatidylcholine at the mercury-electrolyte interface. *Langmuir* **1998**, *14*, 6269–6273.
25. Smaby, J.M.; Brockman, H.L. Surface dipole moments of lipids at the argon-water interface. Similarities among glycerol-ester-based lipids. *Biophys. J.* **1990**, *58*, 195–204.
26. Moncelli, M.R.; Becucci, L. A novel model of the hanging mercury drop electrode. *J. Electroanal. Chem.* **1997**, *433*, 91–96.
27. De Almeida, R.F.M.; Loura, L.M.S.; Fedorov, A.; Prieto, M. Lipid rafts have different sizes depending on membrane composition: A time-resolved fluorescence resonance energy transfer study. *J. Mol. Biol.* **2005**, *346*, 1109–1120.

28. De Almeida, R.F.M.; Loura, L.M.S.; Prieto, M. Membrane lipid domains and rafts: Current applications of fluorescence lifetime spectroscopy and imaging. *Chem. Phys. Lipids* **2009**, *157*, 61–77.

29. Mori, K.; Mahmood, Md.I.; Neya, S.; Matsuzaki, K.; Hoshino, T. Formation of GM1 gangloside clusters on the lipid membrane containing sphingomyelin and cholesterol. *J. Phys. Chem. B* **2012**, *116*, 5111–5121.

30. Terrettaz, S.; Stora, T.; Duschl, C.; Vogel, H. Protein binding to supported lipid membranes: Investigation of the cholera toxin-gangloside interaction by simultaneous impedance spectroscopy and surface plasmon resonance. *Langmuir* **1993**, *9*, 1361–1369.

31. Wang, H.; Pilon, L. Accurate simulations of electric double layer capacitance of ultramicroelectrodes. *J. Phys. Chem. C* **2011**, *115*, 16711–16719.

32. Akimov, S.A.; Hlaponin, E.A.; Bashkirov, P.V.; Boldyrev, I.A.; Mikhalyov, I.I.; Telford, W.G.; Molotkovskaya, I.M. Ganglioside GM1 increases line tension at raft boundary in model membranes. *Biochem. Suppl. Ser. A Membr. Cell Biol.* **2009**, *3*, 216–222.

33. Kycia, A.H.; Wang, J.; Merrill, A.R.; Lipkowski, J. Atomic force microscopy studies of a floating-bilayer lipid membrane on a Au(111) surface modified with a hydrophilic monolayer. *Langmuir* **2011**, *27*, 10867–10877.

34. Thompson, T.E.; Allietta, M.; Brown, R.E.; Johnston, M.L.; Tillack, T.W. Organization of ganglioside G_{M1} in phosphatidylcholine bilayers. *Biochim. Biophys. Acta* **1985**, *817*, 229–237.

35. Bach, D.; Miller, I.R.; Sela, B.-A. Calorimetric studies on various gangliosides and ganglioside-lipid interactions. *Biochim. Biophys. Acta* **1982**, *686*, 233–239.

36. Margheri, G.; D'Agostino, R.; Becucci, L.; Guidelli, R.; Tiribilli, B.; Del Rosso, M. Surface plasmon resonance as detection tool for lipids lateral mobility in biomimetic membranes. *Biomed. Opt. Express* **2012**, *3*, 3119–3126.

37. Ribi, H.O.; Ludwig, D.S.; Mercer, K.L.; Schoolnik, G.K.; Kornberg, R.D. Three-dimensional structure of cholera toxin penetrating a lipid membrane. *Science* **1988**, *239*, 1272–1276.